IEEE Access
Multidisciplinary ⋮ Rapid Review ⋮ Open Access Journal

Received 2 September 2023, accepted 22 September 2023, date of publication 27 September 2023,
date of current version 10 October 2023.

Digital Object Identifier 10.1109/ACCESS.2023.3319293

RESEARCH ARTICLE

Bone Cancer Detection and Classification Using Owl Search Algorithm With Deep Learning on X-Ray Images

EATEDAL ALABDULKREEM[1], MUHAMMAD KASHIF SAEED[2], SAUD S. ALOTAIBI[3], RANDA ALLAFI[4], ABDULLAH MOHAMED[5], AND MANAR AHMED HAMZA[6]

[1]Department of Computer Sciences, College of Computer and Information Sciences, Princess Nourah bint Abdulrahman University, Riyadh 11671, Saudi Arabia
[2]Department of Computer Science, Applied College, Muhayil, King Khalid University, Abha 62529, Saudi Arabia
[3]Department of Information Systems, College of Computing and Information Systems, Umm Al-Qura University, Mecca 24382, Saudi Arabia
[4]Department of Computer and Information Technology, College of Sciences and Arts, Northern Border University, Arar 73213, Saudi Arabia
[5]Research Centre, Future University in Egypt, New Cairo 11845, Egypt
[6]Department of Computer and Self Development, Preparatory Year Deanship, Prince Sattam bin Abdulaziz University, Al-Kharj 16278, Saudi Arabia

Corresponding author: Randa Allafi (Randa.allafi@nbu.edu.sa)

The authors extend their appreciation to the Deanship of Scientific Research at King Khalid University for funding this work through large group Research Project under grant number (RGP2/ 117 /44). Princess Nourah bint Abdulrahman University Researchers Supporting Project number (PNURSP2023R161), Princess Nourah bint Abdulrahman University, Riyadh, Saudi Arabia. The authors extend their appreciation to the Deanship of Scientific Research at Northern Border University, Arar, KSA for funding this research work through the project number NBU-FFR-2023-0115. This study is supported via funding from Prince Sattam bin Abdulaziz University project number (PSAU/2023/R/1444). This study is partially funded by the Future University in Egypt (FUE).

ABSTRACT Bone cancer is treated as a severe health problem, and, in many cases, it causes patient death. Early detection of bone cancer is efficient in reducing the spread of malignant cells and decreasing mortality. Since the manual detection process is a laborious task, it is needed to design an automated system to classify and identify the cancerous bone and the healthy bone. Therefore, this article develops an Owl Search Algorithm with a Deep Learning-Driven Bone Cancer Detection and Classification (OSADL-BCDC) technique. The OSADL-BCDC algorithm follows the principle of transfer learning with a hyperparameter tuning strategy for bone cancer detection. The OSADL-BCDC model employs Inception v3 as a pretrained model for the feature extraction process which does not necessitate a manual segmentation of X-ray images. Besides, the OSA is applied as a hyperparameter optimizer for enhancing the efficacy of the Inception v3 method. Finally, the long short-term memory (LSTM) approach is used for identifying the presence of bone cancer. The proposed OSADL-BCDC technique reduces diagnosis time and achieves faster convergence. The experimental analysis of the OSADL-BCDC algorithm is tested using a set of medical images and the outcomes were measured under different aspects. The comparison study highlighted the improved performance of the OSADL-BCDC model over existing algorithms.

INDEX TERMS Medical imaging, bone cancer, deep learning, artificial intelligence, owl search algorithm.

I. INTRODUCTION

A human body has 206 bones. Bones are generally involved in body muscles and give support to movement. Bone ligaments are fibrous tissues and are full of spongy bone marrow [1]. In recent times, a substantial rise in the number of bone cancers in normal and malignant cancers specifically has been noticed. Even though the proportion of bone malignant cancers was relatively lower than benign ones [2], because of the aggressiveness and comparatively lower survival rate there comes the main issue, irrespective of the technique of medication applied [3]. One such determining component for enhancing functional prognosis was the velocity with the prognosis. A bone tumor arises from the healthier cells and begins to form cancer [4].

Cancer slowly develops and can spread to other parts of the body. This could make bones weaker and damage the bone tissue. As per statics, in the US 3500 public have

The associate editor coordinating the review of this manuscript and approving it for publication was Yudong Zhang.

been affected by bone tumors in 2018, and nearly 47% of bone tumor diagnosed persons became deceased. The clinician prognoses the tumor through various tests. The X-ray image prognosis was mainly utilized for detecting tumors in the bone. The X-ray assimilation rates were distinct for the cancerous bone and healthier bones [5]. Owing to this a tumorous bone image surfaces seem ragged. The severity of bone cancer has been measured by the grade and stage. The cancer growth rate was utilized by physicians for predicting the growth rate of the disease [6]. A prognosis tumor in the bone needs expertise. Bone tumor prognoses are made by a physician manually, which is more time-consuming, and there comes a possibility of error. Detection in the initial stage considers the only element which raises the chances of living of tumor patients.

Developments in artificial intelligence (AI) technology was making innovation in the healthcare analysis of data [7]. Deep learning (DL), a higher-level neural network (NN) resembling the brain of humans, resolves complicated issues that cannot be solved by low-level AI [8]. Convolutional neural network (CNN) techniques portrayed higher performances in examining healthcare images having complicated patterns. The capability of DL in taking two-dimensional medical images was similar to average human experts in the domain [9]. Several researchers have stated extraordinary outcomes in classifying or prognosing a disease with the help of plain MRI, radiography, microscopy, ultrasound, and endoscopy. Similarly, AI technology might be effectively utilized for detecting bone cancers on plain radiographs [10]. When the AI-related classification method executes well in medical practices, human errors, time, and cost, will be dramatically minimized. Although few CNN models are available in the literature, hyperparameter selection is a tedious process. Hyperparameter values considerably affect the performance of the DL models. Since manual trial and error hyperparameter selection is difficult, an automated selection process using metaheuristic algorithms is recommended.

This article develops an Owl Search Algorithm with a Deep Learning-Driven Bone Cancer Detection and Classification (OSADL-BCDC) method. The proposed OSADL-BCDC algorithm proposes to identify the presence of bone cancer from X-ray images by the use of DL models. Particularly, the OSADL-BCDC model employs Inception v3 as a pre-trained model for the feature extraction process which does not necessitate a manual segmentation of the X-ray images. To enhance the efficacy of the Inception v3 model, the OSA is applied as a hyperparameter optimizer. Finally, the long short-term memory (LSTM) method was used for identifying the presence of bone tumors. The experimental analysis of the OSADL-BCDC algorithm is tested using a set of medical images and the outcomes were considered in many aspects. The key contributions of the paper are listed as follows.

- Develop an OSADL-BCDC technique, which combines the DL model, hyperparameter optimization using OSA, and LSTM-based tumor identification to advance the accuracy and efficiency of bone cancer detection and classification from X-ray images. To the best of our knowledge, the proposed OSADL-BCDC technique never existed in the literature.
- OSA is applied to fine-tune the Inception v3 model, enhancing its efficacy in detecting bone cancer from X-ray images. This integration of a metaheuristic optimization technique contributes to improved model performance.
- LSTM is employed to identify the presence of bone tumors in X-ray images, leveraging its sequential modeling capabilities to capture relevant temporal dependencies in the data.

The rest of the paper is organized as follows. Section II provides the related works and section III offers the proposed model. Then, section IV gives the result analysis and section V concludes the paper.

II. RELATED WORKS

Tayebi et al. [11] developed an end-to-end DL-related method for automatic bone marrow cytology. Initiating with bone marrow aspirate digital whole slide images, this system automatically and quickly identifies appropriate areas for cytology, and later classifies and detects every bone marrow cell in all regions. The collective cytomorphological data was captured from a representation named Histogram of Cell Types (HCT) measuring bone marrow cell class probability distribution and serving as cytological patient fingerprints. In [12], the researchers applied various ML techniques for classifying the bone X-ray images of the musculoskeletal radiographs (MURA) dataset as no fracture and fractures category. The 4 distinct classifiers Decision tree (DT), RBF-SVM, Logistic Regression (LR) and linear SVM have been used for abnormality recognition.

In [13], transfer learning (TL) methods, the adoption of pretrained CNNs, to public datasets over osteosarcoma histological images for detecting necrotic images from non-necrotic and healthier tissues. Firstly, the data was pre-processed, and distinct categorizations were implied. Subsequently, TL techniques which include Inception V3 and VGG19 were trained and utilized on Whole Slide Images (WSI) having no patches, to improve the accuracy of the outputs. At last, the methods were applied to distinct classifier issues, adding multi-class and binary classifiers. In [14], the researchers suggest an approach for predicting the malignancy or benignity of bone tumors with the help of DL automatically. They finely tuned ResNet152 and VGG16 trained on ImageNet by making use of image patches derived from 38 plain X-ray images of three patients.

In [15], the authors explain the advancement of a deep CNN for determining the absence or presence of bone metastases. This method comprises 3 sub-networks that focus on extracting, classifying, and aggregating higher-level features in a data-driven way. There were 2 major innovations Firstly, the prognosis was expected by scrutinizing posterior as well

as anterior views that resulted in more precision. Secondly, a spatial attention feature aggregation operator was suggested for improvising spatial location data. In [16], an automated bone tumor recognition system has been suggested to help oncologists in the initial identification of bone tumours and aids them in doing prompt medication. SVM-related Fuzzy C-Means (FCM) and M3-filtered segmentation approaches were recommended for deducting the bone tumors.

Presently, several DL models can be employed in medical image analysis, comprising bone cancer detection, relying on manual hyperparameter tuning. Manual tuning of the hyperparameters can be time-consuming, and resource-intensive, and does not guarantee optimal performance. DL models have a large search space for hyperparameters, making it difficult to discover every probable combination effectually. Proper selection of hyperparameters considerably affects a model's ability to generalize from the training data to unseen data, which is crucial for the reliability of bone cancer detection systems. Inappropriate selection of the hyperparameters can result in model overfitting or underfitting. Therefore, there is a clear research gap in the development and evaluation of automated hyperparameter selection methods specifically tailored to DL models for bone cancer detection and classification. These methods should take into account the unique characteristics of medical image data, including X-rays and bone scans, and aim to improve the accuracy, efficiency, and generalization of bone cancer detection systems while reducing the reliance on manual tuning, making them more accessible to researchers and healthcare professionals.

III. THE PROPOSED BONE CANCER CLASSIFICATION MODEL

In this study, a new OSADL-BCDC method was established for the identification and classification of bone cancer using X-ray images. The proposed OSADL-BCDC method initially performs data augmentation at the pre-processing stage to increase the size of the dataset. In addition, the OSADL-BCDC model employed OSA with Inception v3 as a pretrained model for the feature extraction process. Finally, the LSTM network is used for the classification of X-rays into bone cancer or healthy. Fig. 1 describes the working process of the OSADL-BCDC method.

A. IMAGE PRE-PROCESSING

To increase the effectiveness of DL approaches, a huge group of data was required. However, retrieving the dataset commonly derives from several constraints. Therefore, to overcome the challenges, a data augmentation approach was executed to raise the sample image count from the instance data. Data augmentation methods such as Rotation and Zooming were utilized [17]. The rotation data augmentation approach was implemented from the clockwise direction with an angle of 90 degrees. Moreover, the Zooming augmentation process was executed on image data by obtaining 0.5 and 0.8 zooming factor values. With the imbalance problem, the aforementioned data augmentation system was executed.

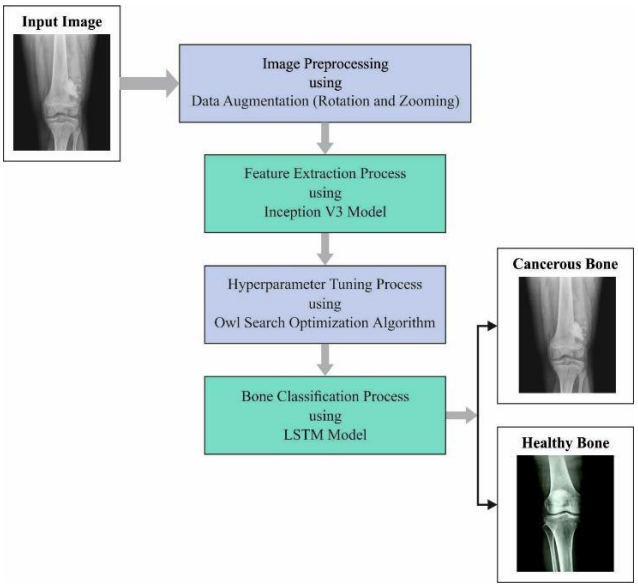

FIGURE 1. Working process of OSADL-BCDC method.

Afterwards utilizing the data augmentation approach the instance data from all the classes were enhanced.

B. FEATURE EXTRACTION

Once the preprocessing stage is completed, the Inception v3 is applied as a pre-trained model for the feature extraction process. CNN is a very commonly utilized technique for analysing visual imagery. CNN is the most common DNN. It is formed of neurons which have learnable weight as well as bias [18]. Additionally, it contains output, input, and hidden layers. During all feed-forward neural networks (FFNNs), some middle layer was named as hidden, conversely, in CNN, one or more hidden layers are executed convolutional. Besides, the CNNs are 2 important elements:

- The Hidden layer/Feature extracting part: During this part, the network executes a series of convolutional and pooling functions in which the feature was identified.
- The Classification part: At this point, the fully connected (FC) layers serve as classification on top of these removed features allocating a probability to forecast objects on images.

Furthermore, it can be utilized 3 important kinds of layers for building ConvNet structures namely pooling, convolutional, and FC Layers:

- Input layer: CNN's proceeds benefit from the detail that input contains images and it constrains the structure in a further sensible manner. Especially, different from a regular NN, the layer of ConvNet has neurons decided in 3 dimensional like height, depth, and width, whereas depth was usually the count of colour channels utilized (HSV $= 3$, RGB $= 3$, CYMK $= 4$,).
- The convolutional layer is the fundamental component of CNNs. It creates the feature map also named an activation map utilizing the feature detectors. The feature detector also called a kernel or filter, interchanges across the receptive field

of images, verifying if the feature is present. Besides, the 1st layers distinguish fundamental features like horizontal as well as vertical edges, but the next layer removes further difficult features. This procedure was recognized as convolutional. The feature detector is the 2D array of weights that signifies the part of the images. But, it differs in size, the filter size was classically a 3×3 matrix. The most popular activation function utilized during this layer is ReLU.

• Pooling layer: conducts dimensionality decrease, with decreasing the number of parameters from the input. The kernel executes an aggregation function to value in the receptive region and populates the resultant array. Two types of pooling exist namely max-pooling and avg pooling. The max-pooling chooses the pixel with the maximal value for sending to the resultant array, but the average pooling computes the average value in the receptive region for sending to the resultant arrays.

• Fully connected layer: During the FC layer, all the nodes from the resultant layer attach directly to nodes from the preceding layer. This layer executes the task of classifier dependent upon the feature extraction with the preceding layer and its distinct filters. The classifier layer provides a group of confidence scores utilizing commonly softmax and sigmoid activation functions. The Inception V3 is a DL approach dependent upon CNN that was utilized as an image classifier [19]. The InceptionV3 is a higher version of the fundamental model Inception V1 that was established by GoogLeNet in 2014. The inception V3 was just the advanced and optimized version of the inception V1 method. The Inception V3 method utilized many approaches to optimize the network to superior method adaptation.

An inception element utilized 1×1, 3×3, and 5×5 convolution layers simultaneously, afterwards concatenated 3 types of outcomes and communicated them to the next element. In this manner, it is assumed data of distinct scales together with improving the width of networks. Besides, an inception element also is divided channel-wise as well as spatial-wise correlation and the smaller size of the convolutional kernel significantly decreases the parameter. Using the Inception element, Inception-v3 exchanged the 5×5 convolutional layer from the original Inception network with two 3×3 convolutional layers to decrease the count of parameters but maintain the receptive field and improve the capability of representations. Besides, another innovation of Inception-v3 has to decompose a huge $n \times n$ convolutional kernel (i.e., a 7×7 convolutional kernel) as two 1D convolutional kernels with sizes of $n \times 1$ and $1 \times n$ correspondingly. It can improve the model's nonlinear representation ability but decrease the risk of over-fitting.

C. HYPERPARAMETER OPTIMIZATION

In this study, the OSA is utilized as a hyperparameter optimizer of the InceptionV3 architecture. The OSA begins with n amount of population, named owls that is, an early guess for the problem solution [20]. Here, the forest is regarded as a d dimension-searching space. Regarding owls in the forest, the first location for owls is saved in $n \times d$ matrixes,

$$0 = \begin{bmatrix} O_{1,1} & \cdots & O_{1,d} \\ \vdots & \ddots & \vdots \\ O_{n,1} & \cdots & O_{n,d} \end{bmatrix} \tag{1}$$

In Eq. (1), the element $O_{i,j}$ in the matrix determines the j^{th} parameter (dimension) of i^{th} owls.

Then, the early owls were normalized to provide a uniformly distributed location using the subsequent equation:

$$0_i = 0_l + (O_l + O_u) \times U\,(0, 1) \tag{2}$$

where $0 \leq U\,(0, 1) \leq 1$ defines a uniform distribution of arbitrary numbers, and $O_i \in [O_l, O_u]$.

The cost for the location of the owls in a forest is estimated according to the cost function and saved in a matrix in the following:

$$f = \begin{bmatrix} f_1\left(\left[O_{1,1}, O_{1,2}, \ldots O_{1,d}\right]\right) \\ \vdots \\ f_n\left(\left[O_{n,1}, O_{n,2}, \ldots O_{n,d}\right]\right) \end{bmatrix} \tag{3}$$

The cost value of location for the owls is directly based on the intensity data received by the ears. Thus, maximal intensity can be accomplished using the optimal owl since it is very close to prey. The intensity value data of i^{th} owls is applied for updating the location in the following:

$$I_i = \frac{f_i - f_m^1}{f_m^h - f_m^1} \tag{4}$$

where,

$$f_m^h = \max_{m \in 1, \ldots n} f_m \tag{5}$$

and,

$$f_m^1 = \min_{m \in 1, \ldots n} f_m \tag{6}$$

Next, the distance data for the owls and prey population can be accomplished by:

$$D_i = \sqrt{\sum\nolimits_i (O_i - L)^2} \tag{7}$$

In Eq. (7), L defines the location of the prey that is accomplished using the best owl.

The concept is that there is one prey as a global optimal in the forest. In the hunting procedure, owls flight silent toward the prey so that intensity changes for $i - th$ owls are regarded in the following:

$$C_i = \frac{I_i}{A_i^2} + N_r \tag{8}$$

In Eq. (8), A_i^2 characterizes the simulated rather than $4\pi D_i^2$, and N_r defines the random noise.

The owls have to change the location to silent as per the prey movement. According to probability, the OSA models the prey movement as follows:

$$0_i^{t+1} = \begin{cases} O_i^t + \beta \times C_i \times |\alpha L - O_i^t|, & p_{pm} < 0.5 \\ O_i^t - \beta \times C_i \times |\alpha L - O_i^t|, & p_{pm} \geq 0.5 \end{cases} \quad (9)$$

In Eq. (9), p_{pm} signifies the probability of prey movement, $0 \leq \alpha \leq 0.5$ defines the uniform distribution arbitrary number, and $0 \leq \beta \leq 1.9$ denotes a linearly reducing continuously.

The β coefficient comprises the exploration in the searching space which makes them reliable when compared to the other bio-inspired algorithms. The OSA technique devises a fitness function (FF) for accomplishing maximal classifier performance. It solves a positive integer for indicating the better efficiency of candidate results. In such cases, the reduced classifier error rate was assumed that FF is given as follows:

$$\begin{aligned} fitness\,(x_i) &= Classifier\ Error\ Rate\,(x_i) \\ &= \frac{number\ of\ misclassified\ samples}{Total\ number\ of\ samples} * 100 \end{aligned} \quad (10)$$

D. BONE CANCER CLASSIFICATION

Finally, the LSTM network is used for the classification of X-rays for bone cancer or normal. LSTM is a variant of RNN with an improved function for computing the hidden state [21]. The LSTM for resolving the long-term dependency issue with added to the gate procedure. As demonstrated in Fig. 2, the LSTM cell utilizes the model of the gate for determining that data for keeping or erasing in the memory. The gate is a process for transferring required data selectively. It can be attained by creating a group of current inputs, memory, and preceding states. The LSTM has 3 gates. An output, input, and forget gates. The forget gate was responsible for selecting that information for remembering and that to throw away. This decision was developed with the sigmoid layer as represented in Eq. (11).

$$f_t = \sigma\left(x_t W^f + h_{t-1} U^f\right) \quad (11)$$

The output is 0 or 1, whereas 0 refers to forget and 1 signifies the keep. The second gate is the input gate.

Another sigmoid layer was utilized for determining the value that was upgraded as demonstrated in Eq. (12).

$$i_t = \sigma\left(x_t W^i + h_{t-1} U^i\right) \quad (12)$$

The *tanh* function generates the vector of candidates which is additional to the state as demonstrated in Eq. (13).

$$\hat{C}_t = \tanh\left(x_t W^g + h_{t-1} U^g\right) \quad (13)$$

Afterwards, the LSTM upgrades the old cell state C_{t-1} that C_t as represented in Eq. (14).

$$C_t = \sigma\left(f_t \times C_{t-1} + i_t \times \hat{C}_t\right) \quad (14)$$

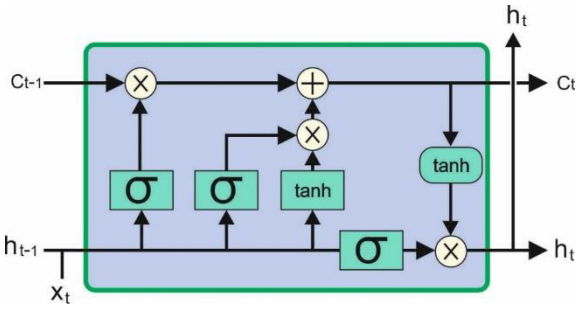

FIGURE 2. Structure of LSTM.

FIGURE 3. Sample images.

TABLE 1. Details of datasets.

Class Name	No. of Instances
Cancerous	100
Healthy	100
Total No. of Instances	200

Eventually, during the output gate, the LSTM utilizes a sigmoid function for determining which part of cell states appear in Eq. (15).

$$o_t = \sigma\left(x_t W^o + h_{t-1} U^o\right) \quad (15)$$

In Eq. (16), multiplying 0_t by $\tanh(C_t)$ can implicitly define that part to eliminate.

$$h_t = \tanh\left(C_t\right) \times 0_t \quad (16)$$

IV. RESULTS AND DISCUSSION

The proposed model is simulated using Python 3.6.5 tool on PC i5-8600k, GeForce 1050Ti 4GB, 16GB RAM, 250GB SSD, and 1TB HDD. The parameter settings are given as follows: learning rate: 0.01, dropout: 0.5, batch size: 5, epoch count: 50, and activation: ReLU. The performance analysis of the OSADL-BCDC algorithm is tested using a set of X-ray images gathered from various sources like The TCIA (Cancer

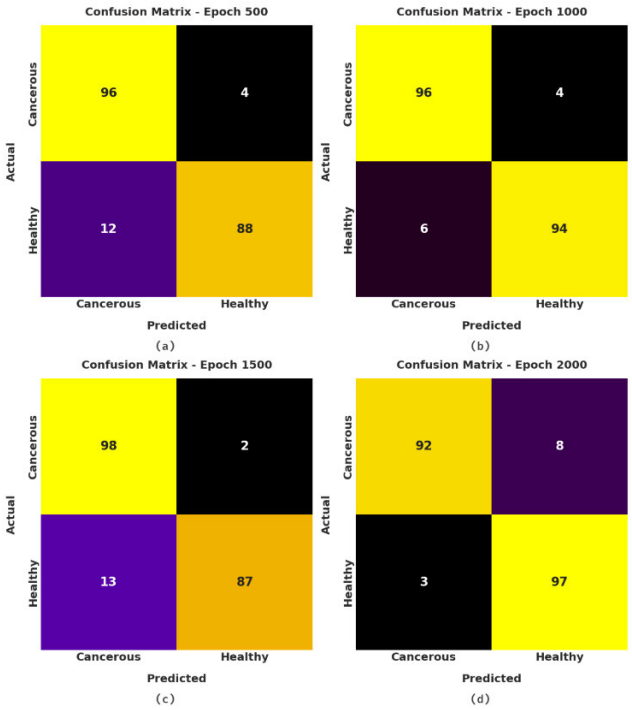

FIGURE 4. Confusion matrices of OSADL-BCDC method (a) Epoch 500, (b) Epoch 1000, (a) Epoch 1500, and (d) Epoch 2000.

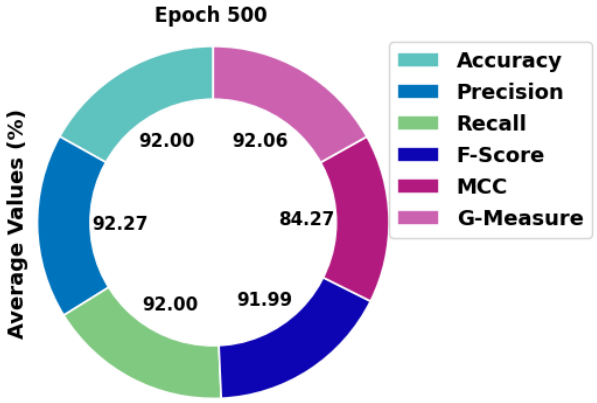

FIGURE 5. Average analysis of OSADL-BCDC method under epoch 500.

Imaging Archive), and the Indian Institute of Engineering Science and Technology, Shibpur (IIEST). In this study, a set of 200 images is taken with 100 images under the cancerous class and 100 images under the healthy classes as shown in Table 1. A few sample images are illustrated in Fig. 3.

Fig. 4 highlights the confusion matrices created by the OSADL-BCDC algorithm under dissimilar epochs. With 500 epochs, the OSADL-BCDC technique has detected 96 instances in the cancerous class and 88 instances in the healthy class. Also, with 1000 epochs, the OSADL-BCDC methodology has detected 96 instances in the cancerous class and 94 instances in the healthy class. In line, with 1500 epochs, the OSADL-BCDC system has detected 98 instances in the cancerous class and 87 instances in the

TABLE 2. Result analysis of OSADL-BCDC approach with different measures and epochs.

Class Labels	$Accu_y$	$Prec_n$	$Reca_l$	F_{score}	MCC	$G_{measure}$
Epoch-500						
Cancerous	92.00	88.89	96.00	92.31	84.27	92.38
Healthy	92.00	95.65	88.00	91.67	84.27	91.75
Average	92.00	92.27	92.00	91.99	84.27	92.06
Epoch-1000						
Cancerous	95.00	94.12	96.00	95.05	90.02	95.05
Healthy	95.00	95.92	94.00	94.95	90.02	94.95
Average	95.00	95.02	95.00	95.00	90.02	95.00
Epoch-1500						
Cancerous	92.50	88.29	98.00	92.89	85.52	93.02
Healthy	92.50	97.75	87.00	92.06	85.52	92.22
Average	92.50	93.02	92.50	92.48	85.52	92.62
Epoch-2000						
Cancerous	94.50	96.84	92.00	94.36	89.11	94.39
Healthy	94.50	92.38	97.00	94.63	89.11	94.66
Average	94.50	94.61	94.50	94.50	89.11	94.53

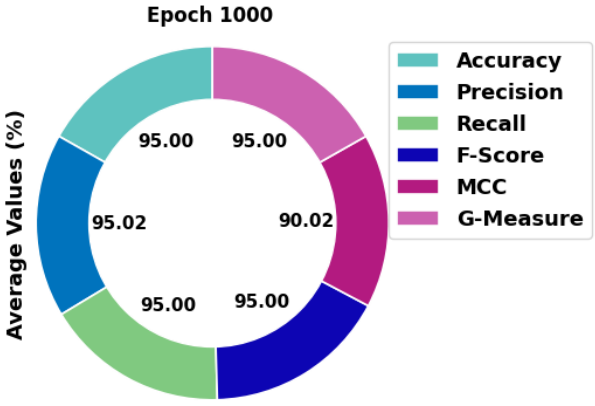

FIGURE 6. Average analysis of OSADL-BCDC method under epoch 1000.

healthy class. Besides, with 2000 epochs, the OSADL-BCDC approach has detected 92 instances in the cancerous class and 97 instances in the healthy class.

Table 2 offers the overall bone cancer classification results of the OSADL-BCDC model under distinct epochs. Fig. 5 illustrates a brief bone cancer classifier outcome of the OSADL-BCDC model with 500 epochs. The OSADL-BCDC approach has detected the images under cancerous class with $accu_y$ of 92%, $prec_n$ of 88.89%, $reca_l$ of 96%, F_{score} of 92.31%, MCC of 84.27%, and $G_{measure}$ of 91.75%. Concurrently, the OSADL-BCDC method has detected the images under healthy class with $accu_y$ of 92%, $prec_n$ of

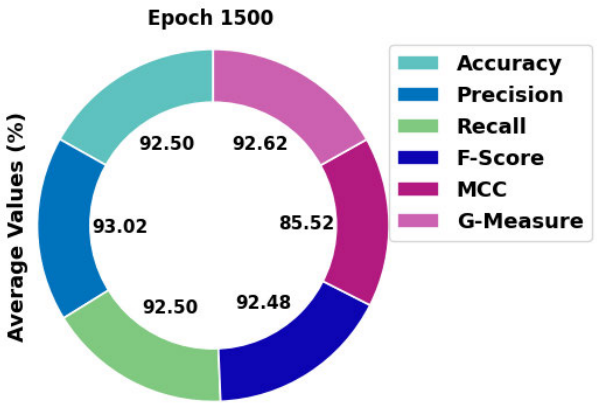

FIGURE 7. Average analysis of OSADL-BCDC method under epoch 1500.

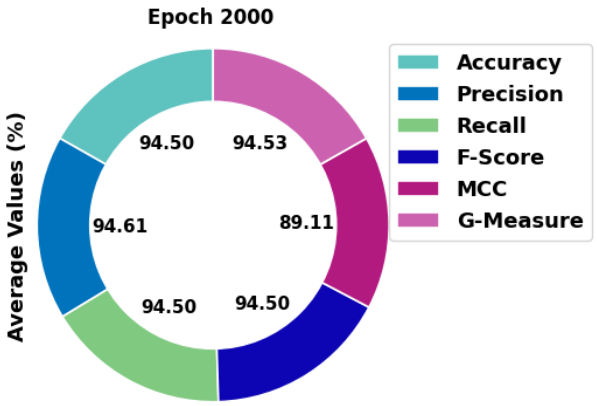

FIGURE 8. Average analysis of OSADL-BCDC method under epoch 2000.

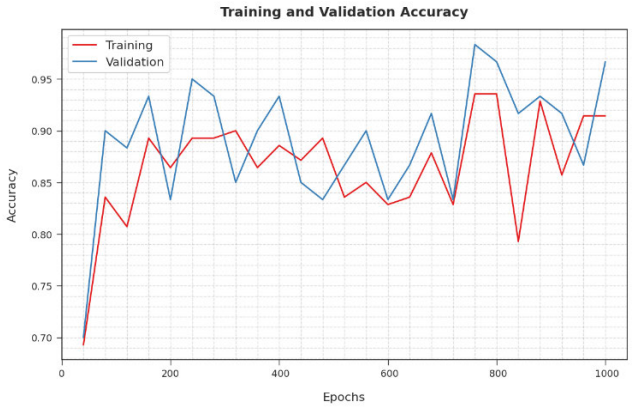

FIGURE 9. TA and VA analysis of the OSADL-BCDC approach.

95.65%, $reca_l$ of 88%, F_{score} of 91.67%, MCC of 84.27%, and $G_{measure}$ of 91.75%.

Fig. 6 depicts a detailed bone cancer classifier outcome of the OSADL-BCDC approach with 100 epochs. The OSADL-BCDC system has detected the images under cancerous class with $accu_y$ of 95%, $prec_n$ of 94.12%, $reca_l$ of 96%, F_{score} of 95.05%, MCC of 90.02%, and $G_{measure}$ of

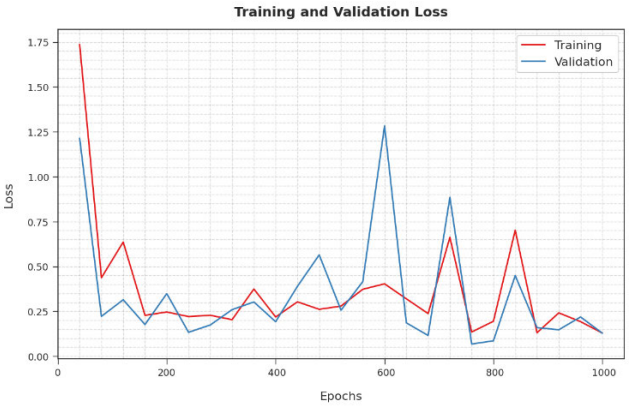

FIGURE 10. TL and VL analysis of the OSADL-BCDC method.

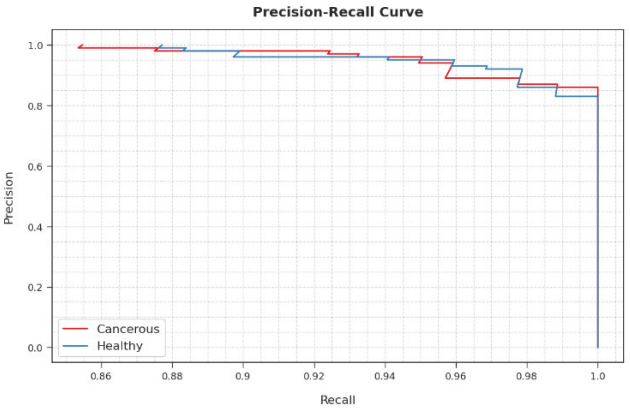

FIGURE 11. Precision-recall (PR) curve analysis of OSADL-BCDC method.

95.05%. Simultaneously, the OSADL-BCDC methodology has detected the images under healthy class with $accu_y$ of 95%, $prec_n$ of 95.92%, $reca_l$ of 94%, F_{score} of 94.95%, MCC of 90.02%, and $G_{measure}$ of 94.95%.

Fig. 7 showcases a brief bone cancer classifier outcome of the OSADL-BCDC algorithm with 1500 epochs. The OSADL-BCDC approach has detected the images under cancerous class with $accu_y$ of 92.50%, $prec_n$ of 88.29%, $reca_l$ of 98%, F_{score} of 92.89%, MCC of 85.52%, and $G_{measure}$ of 93.02%. Followed by, the OSADL-BCDC method has detected the images under healthy class with $accu_y$ of 92.50%, $prec_n$ of 97.75%, $reca_l$ of 87%, F_{score} of 92.06%, MCC of 85.52%, and $G_{measure}$ of 92.22%.

Fig. 8 demonstrates a detailed bone cancer classifier outcome of the OSADL-BCDC methodology with 2000 epochs. The OSADL-BCDC system has detected the images under cancerous class with $accu_y$ of 94.50%, $prec_n$ of 96.84%, $reca_l$ of 92%, F_{score} of 94.36%, MCC of 89.11%, and $G_{measure}$ of 94.39%. Likewise, the OSADL-BCDC algorithm has detected the images under healthy class with $accu_y$ of 94.50%, $prec_n$ of 92.38%, $reca_l$ of 97%, F_{score} of 94.63%, MCC of 89.11%, and $G_{measure}$ of 94.66%.

The training accuracy (TA) and validation accuracy (VA) gained by the OSADL-BCDC approach on the test dataset are illustrated in Fig. 9. The outcomes represented that the

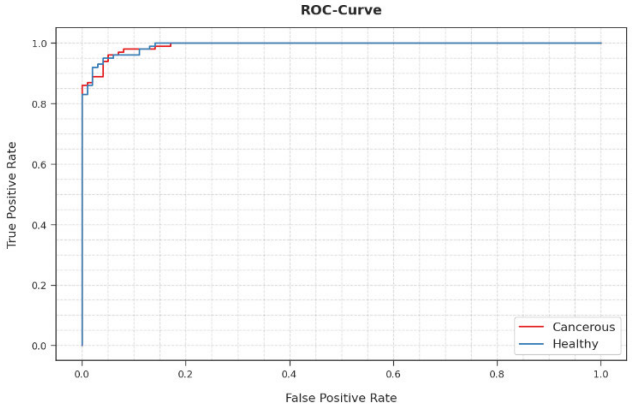

FIGURE 12. ROC curve analysis of the OSADL-BCDC method.

TABLE 3. Comparison study of the OSADL-BCDC approach with recent methodologies.

Methods	$Accu_y$	$Prec_n$	$Reca_l$	F_{score}
OSADL-BCDC	95.00	95.02	95.00	95.00
Random Forest Model	69.05	75.69	79.07	77.71
SVM Model	92.59	90.63	93.58	93.13
BCDFE-ML Model	92.48	92.70	89.17	93.83
ResNet50 Model	82.57	81.02	78.92	81.75
Inception v3 Model	83.33	81.48	89.74	78.10
Efficient-Net Model	85.79	82.28	91.53	83.61

OSADL-BCDC method obtained the highest values of TA and VA. The VA seemed to be better than the TA.

The training loss (TL) and validation loss (VL) accomplished by the OSADL-BCDC technique on the test dataset are shown in Fig. 10. The outcomes exposed that the OSADL-BCDC method attained minimum values of TL and VL. Especially, the VL seemed to be lesser than TL.

A detailed PR inspection of the OSADL-BCDC system on the test dataset is revealed in Fig. 11. From the figure, it is noted that the OSADL-BCDC model has obtained maximal PR performance under all classes.

A comprehensive ROC examination of the OSADL-BCDC method on the test dataset is described in Fig. 12. The outcomes showed that the OSADL-BCDC technique has shown its capability in classifying two dissimilar classes on the test dataset.

Table 3 reports an overall comparison analysis of the OSADL-BCDC method with other DL techniques [22], [23]. Fig. 13 showcases the comparative $accu_y$ and $F1_{score}$ examination of the OSADL-BCDC method with recent approaches.

The outcomes indicated that the OSADL-BCDC method has shown better outcomes than existing techniques. Concerning $accu_y$, the OSADL-BCDC technique has offered an increased $accu_y$ of 95% whereas the RF, SVM, BCDFE-ML, ResNet50, Inception v3, and EfficientNet models have obtained reduced $accu_y$ of 69.05%, 92.59%, 92.48%, 82.57%, 83.33%, and 85.79% respectively. Besides, about $F1_{score}$, the OSADL-BCDC approach has obtainable a higher $F1_{score}$ of 95% whereas the RF, SVM, BCDFE-

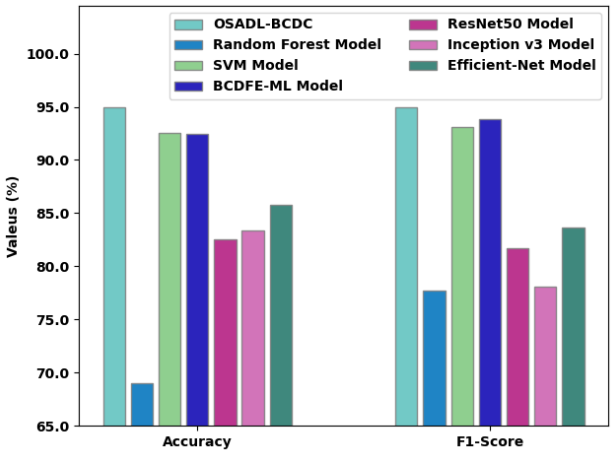

FIGURE 13. $Accu_y$ and $F1_{score}$ analysis of OSADL-BCDC approach with recent methodologies.

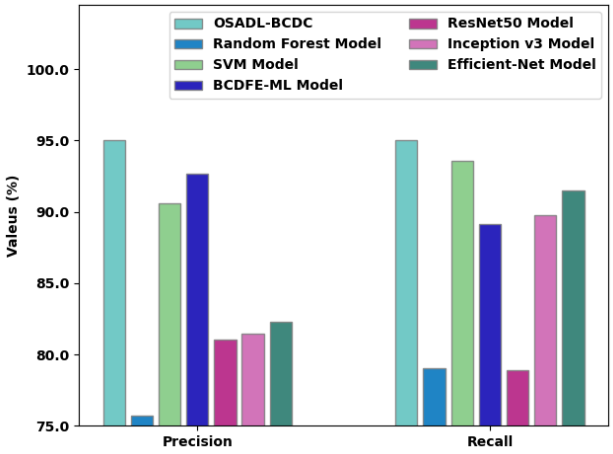

FIGURE 14. $Prec_n$ and $Reca_l$ analysis of OSADL-BCDC approach with recent methodologies.

ML, ResNet50, Inception v3, and EfficientNet methods have obtained a lesser $F1_{score}$ of 77.71%, 93.13%, 93.83%, 81.75%, 78.10%, and 83.61% correspondingly.

Fig. 14 depicts the comparative $prec_n$ and $reca_l$ examination of the OSADL-BCDC method with recent techniques. The outcomes represented that the OSADL-BCDC approach has demonstrated optimum outcomes over existing methods. In terms of $prec_n$, the OSADL-BCDC method has offered a maximal $prec_n$ of 95.02% whereas the RF, SVM, BCDFE-ML, ResNet50, Inception v3, and EfficientNet systems have obtained reduced $prec_n$ of 75.69%, 90.63%, 92.70%, 81.02%, 81.48%, and 82.28% correspondingly.

Moreover, concerning $reca_l$, the OSADL-BCDC methodology has accessible superior $reca_l$ of 95% whereas the RF, SVM, BCDFE-ML, ResNet50, Inception v3, and Efficient-Net algorithms have attained decreased $reca_l$ of 79.07%, 93.58%, 89.17%, 78.92%, 89.74%, and 91.53% correspondingly. From the detailed outcomes and discussion, it is assumed that the OSADL-BCDC method has obtained the highest bone cancer classification performance over other techniques.

V. CONCLUSION

In this study, a novel OSADL-BCDC method was established for the identification and classification of bone cancer utilizing X-ray images. The proposed OSADL-BCDC approach initially performs data augmentation at the pre-processing stage to increase the size of the dataset. In addition, the OSADL-BCDC model employed OSA with Inception v3 as a pretrained model for the feature extraction process. At last, the LSTM network is used for the classification of X-rays into bone cancer or healthy. The utilization of the pre-trained model for the feature extraction process does not necessitate a manual segmentation of the X-ray images. In addition, the presented OSADL-BCDC model reduces diagnosis time and achieves faster convergence. The experimental analysis of the OSADL-BCDC method is tested using a set of medical images and the outcomes were measured under different aspects. The comparison study highlighted the improved performance of the OSADL-BCDC technique over recent state of art methods with maximum accuracy of 95%. In the future, deep instance segmentation techniques can be exploited to boost the classifier performance. Future work can focus on the design of explainable artificial intelligence models for bone cancer detection to gain trust and acceptance in clinical practice. Besides, future work can concentrate on the integration of many imaging modalities, such as X-rays, MRI, CT scans, and PET scans to offer a highly comprehensive view of bone cancer.

VI. ACKNOWLEDGMENT

The authors extend their appreciation to the Deanship of Scientific Research at King Khalid University for funding this work through large group Research Project under grant number (RGP2/ 117 /44). Princess Nourah bint Abdulrahman University Researchers Supporting Project number (PNURSP2023R161), Princess Nourah bint Abdulrahman University, Riyadh, Saudi Arabia. The authors extend their appreciation to the Deanship of Scientific Research at Northern Border University, Arar, KSA for funding this research work through the project number NBU-FFR-2023-0115. This study is supported via funding from Prince Sattam bin Abdulaziz University project number (PSAU/2023/R/1444). This study is partially funded by the Future University in Egypt (FUE).

REFERENCES

[1] A. Ratley, J. Minj, and P. Patre, "Leukemia disease detection and classification using machine learning approaches: A review," in *Proc. 1st Int. Conf. Power, Control Comput. Technol. (ICPC2T)*, Jan. 2020, pp. 161–165.

[2] M. W. Nadeem, H. G. Goh, A. Ali, M. Hussain, M. A. Khan, and V. A. P. Ponnusamy, "Bone age assessment empowered with deep learning: A survey, open research challenges and future directions," *Diagnostics*, vol. 10, no. 10, p. 781, 2020.

[3] D. Shrivastava, S. Sanyal, A. K. Maji, and D. Kandar, "Bone cancer detection using machine learning techniques," in *Smart Healthcare for Disease Diagnosis and Prevention*. New York, NY, USA: Academic Press, 2020, pp. 175–183.

[4] H. B. Arunachalam, R. Mishra, O. Daescu, K. Cederberg, D. Rakheja, A. Sengupta, D. Leonard, R. Hallac, and P. Leavey, "Viable and necrotic tumor assessment from whole slide images of osteosarcoma using machine-learning and deep-learning models," *PLoS ONE*, vol. 14, no. 4, Apr. 2019, Art. no. e0210706.

[5] F. R. Eweje, B. Bao, J. Wu, D. Dalal, W.-H. Liao, Y. He, Y. Luo, S. Lu, P. Zhang, X. Peng, R. Sebro, H. X. Bai, and L. States, "Deep learning for classification of bone lesions on routine MRI," *EBioMedicine*, vol. 68, Jun. 2021, Art. no. 103402.

[6] Y. He, I. Pan, B. Bao, K. Halsey, M. Chang, H. Liu, S. Peng, R. A. Sebro, J. Guan, T. Yi, A. T. Delworth, F. Eweje, L. J. States, P. J. Zhang, Z. Zhang, J. Wu, X. Peng, and H. X. Bai, "Deep learning-based classification of primary bone tumors on radiographs: A preliminary study," *eBioMedicine*, vol. 62, Dec. 2020, Art. no. 103121.

[7] C. E. von Schacky, N. J. Wilhelm, V. S. Schäfer, Y. Leonhardt, F. G. Gassert, S. C. Foreman, F. T. Gassert, M. Jung, P. M. Jungmann, M. F. Russe, C. Mogler, C. Knebel, R. von Eisenhart-Rothe, M. R. Makowski, K. Woertler, R. Burgkart, and A. S. Gersing, "Multitask deep learning for segmentation and classification of primary bone tumors on radiographs," *Radiology*, vol. 301, no. 2, pp. 398–406, Nov. 2021.

[8] N. Papandrianos, E. Papageorgiou, A. Anagnostis, and K. Papageorgiou, "Bone metastasis classification using whole body images from prostate cancer patients based on convolutional neural networks application," *PLoS ONE*, vol. 15, no. 8, Aug. 2020, Art. no. e0237213.

[9] D. Pan, R. Liu, B. Zheng, J. Yuan, H. Zeng, Z. He, Z. Luo, G. Qin, and W. Chen, "Using machine learning to unravel the value of radiographic features for the classification of bone tumors," *BioMed Res. Int.*, vol. 2021, pp. 1–10, Mar. 2021.

[10] S. Gitto, R. Cuocolo, K. van Langevelde, M. A. J. van de Sande, A. Parafioriti, A. Luzzati, M. Imbriaco, L. M. Sconfienza, and J. L. Bloem, "MRI radiomics-based machine learning classification of atypical cartilaginous tumour and grade II chondrosarcoma of long bones," *eBioMedicine*, vol. 75, Jan. 2022, Art. no. 103757.

[11] R. M. Tayebi, Y. Mu, T. Dehkharghanian, C. Ross, M. Sur, R. Foley, H. R. Tizhoosh, and C. J. V. Campbell, "Automated bone marrow cytology using deep learning to generate a histogram of cell types," *Commun. Med.*, vol. 2, no. 1, pp. 1–14, Apr. 2022.

[12] P. K. Mall, P. K. Singh, and D. Yadav, "GLCM based feature extraction and medical X-ray image classification using machine learning techniques," in *Proc. IEEE Conf. Inf. Commun. Technol.*, Dec. 2019, pp. 1–6.

[13] D. M. Anisuzzaman, H. Barzekar, L. Tong, J. Luo, and Z. Yu, "A deep learning study on osteosarcoma detection from histological images," *Biomed. Signal Process. Control*, vol. 69, Aug. 2021, Art. no. 102931.

[14] K. Furuo, K. Morita, T. Hagi, T. Nakamura, and T. Wakabayashi, "Automatic benign and malignant estimation of bone tumors using deep learning," in *Proc. 5th IEEE Int. Conf. Cybern. (CYBCONF)*, Jun. 2021, pp. 030–033.

[15] Y. Pi, Z. Zhao, Y. Xiang, Y. Li, H. Cai, and Z. Yi, "Automated diagnosis of bone metastasis based on multi-view bone scans using attention-augmented deep neural networks," *Med. Image Anal.*, vol. 65, Oct. 2020, Art. no. 101784.

[16] B. Jabber, M. Shankar, P. V. Rao, A. Krishna, and C. Z. Basha, "SVM model based computerized bone cancer detection," in *Proc. 4th Int. Conf. Electron., Commun. Aerosp. Technol. (ICECA)*, Nov. 2020, pp. 407–411.

[17] P. Dai, Y. Li, H. Zhang, J. Li, and X. Cao, "Accurate scene text detection via scale-aware data augmentation and shape similarity constraint," *IEEE Trans. Multimedia*, vol. 24, pp. 1883–1895, 2022.

[18] M. A. Hossain and M. M. Ali, "Recognition of handwritten digits using convolutional neural network (CNN)," *Global J. Comput. Sci. Technol.*, 2019.

[19] C. Wang, D. Chen, L. Hao, X. Liu, Y. Zeng, J. Chen, and G. Zhang, "Pulmonary image classification based on inception-v3 transfer learning model," *IEEE Access*, vol. 7, pp. 146533–146541, 2019.

[20] Y. Cao, Q. Wang, Z. Wang, K. Jermsittiparsert, and M. Shafiee, "A new optimized configuration for capacity and operation improvement of CCHP system based on developed owl search algorithm," *Energy Rep.*, vol. 6, pp. 315–324, Nov. 2020.

[21] P. Liu, X. Qiu, X. Chen, S. Wu, and X. Huang, "Multi-timescale long short-term memory neural network for modelling sentences and documents," in *Proc. Conf. Empirical Methods Natural Lang. Process.*, 2015, pp. 2326–2335.

[22] A. Sharma, D. P. Yadav, H. Garg, M. Kumar, B. Sharma, and D. Koundal, "Bone cancer detection using feature extraction based machine learning model," *Comput. Math. Methods Med.*, vol. 2021, pp. 1–13, Dec. 2021.

[23] C.-W. Park, S.-J. Oh, K.-S. Kim, M.-C. Jang, I. S. Kim, Y.-K. Lee, M. J. Chung, B. H. Cho, and S.-W. Seo, "Artificial intelligence-based classification of bone tumors in the proximal femur on plain radiographs: System development and validation," *PLoS ONE*, vol. 17, no. 2, Feb. 2022, Art. no. e0264140.